


RESEARCH ARTICLE

Noninvasive platelet membrane-coated Fe₃O₄ nanoparticles identify vulnerable atherosclerotic plaques

Yuyu Li^{1,2} | Yujie Wang³ | Zequn Xia⁴ | Yangjing Xie^{1,5} | Daozheng Ke¹ | Bing Song¹ | Dan Mu^{3,6} | Ronghui Yu¹ | Jun Xie^{1,4} 

¹Department of Cardiology, National Cardiovascular Disease Regional Center for Anhui, the First Affiliated Hospital of Anhui Medical University, Hefei, China

²Beijing Institute of Heart, Lung, and Blood Vessel Diseases, Beijing Anzhen Hospital Affiliated to Capital Medical University, Beijing, China

³Department of Radiology, Nanjing Drum Tower Hospital, Affiliated Hospital of Medical School, Nanjing University, Nanjing, China

⁴Department of Cardiology, Nanjing Drum Tower Hospital, Affiliated Hospital of Medical School, Nanjing University, Nanjing, China

⁵Department of Medicine, Cardiovascular Center, Medical College of Wisconsin, Milwaukee, Wisconsin, USA

⁶Department of Radiology, Nanjing Drum Tower Hospital Clinical College of Jiangsu University, Nanjing, China

Correspondence

Jun Xie and Ronghui Yu, Department of Cardiology, National Cardiovascular Disease Regional Center for Anhui, the First Affiliated Hospital of Anhui Medical University, No. 218 Jixi Road, Hefei, Anhui 230022, China.
Email: xiejun@ahmu.edu.cn and ronghuiyu@vip.sina.com

Dan Mu, Department of Radiology, Nanjing Drum Tower Hospital, Affiliated Hospital of Medical School, Nanjing University, No. 321 Zhongshan Road, Nanjing 210008, China.
Email: mudan118@126.com

Abstract

Vulnerable atherosclerotic plaques serve as the primary pathological basis for fatal cardiovascular and cerebrovascular diseases. The precise identification and treatment of these vulnerable plaques hold paramount clinical importance in mitigating the incidence of myocardial infarction and stroke. Nevertheless, the identification of vulnerable plaques within the diffuse atherosclerotic plaques dispersed throughout the systemic circulation continues to pose a substantial challenge in clinical practice. Double emulsion solvent evaporation method, specifically the water-in-oil-in-water (W/O/W) technique, was employed to fabricate Fe₃O₄-based poly (lactic-co-glycolic acid) (PLGA) nanoparticles (Fe₃O₄@PLGA). Platelet membranes (PM) were extracted through hypotonic lysis, followed by ultrasound-assisted encapsulation onto the surface of Fe₃O₄@PLGA, resulting in the formation of PM-coated Fe₃O₄ nanoparticles (PM/Fe₃O₄@PLGA). Characterization of PM/Fe₃O₄@PLGA involved the use of dynamic light scattering, transmission electron microscopy, western blotting, and magnetic resonance imaging (MRI). A model of atherosclerotic vulnerable plaques was constructed by carotid artery coarctation and a high-fat diet fed to ApoE^{-/-} (Apolipoprotein E knockout) mice. Immunofluorescence and MRI techniques were employed to verify the functionality of PM/Fe₃O₄@PLGA. In this study, we initially synthesized Fe₃O₄@PLGA as the core material. Subsequently, a platelet membrane was employed as a coating for the Fe₃O₄@PLGA, aiming to enable the detection of vulnerable atherosclerotic plaques through MRI. In vitro, PM/Fe₃O₄@PLGA not only exhibited excellent biosafety but also showed targeted collagen characteristics and MR imaging performance. In vivo, the adhesion of PM/Fe₃O₄@PLGA to atherosclerotic lesions was confirmed in a mouse model of vulnerable atherosclerotic plaques. Simultaneously, PM/Fe₃O₄@PLGA as a novel contrast agent for MRI has shown effective identification of vulnerable atherosclerotic plaques. In terms of safety profile in vivo, PM/Fe₃O₄@PLGA

This is an open access article under the terms of the [Creative Commons Attribution](https://creativecommons.org/licenses/by/4.0/) License, which permits use, distribution and reproduction in any medium, provided the original work is properly cited.

© 2024 The Authors. *Smart Medicine* published by Wiley-VCH GmbH on behalf of Wenzhou Institute, University of Chinese Academy of Sciences.

has not demonstrated significant organ toxicity or inflammatory response in the bloodstream. In this study, we successfully developed a platelet-membrane-coated nanoparticle system for the targeted delivery of Fe₃O₄@PLGA to vulnerable atherosclerotic plaques. This innovative system allows for the visualization of vulnerable plaques using MRI, thereby demonstrating its potential for enhancing the clinical diagnosis of vulnerable atherosclerotic plaques.

KEYWORDS

Fe₃O₄nanoparticle, MRI, platelet membrane, vulnerable atherosclerosis plaques

1 | INTRODUCTION

Ischemic cardiovascular and cerebrovascular diseases, primarily attributed to the rupture of vulnerable atherosclerotic plaques, remain the leading cause of mortality worldwide.¹⁻⁴ Vulnerable plaques are atheromatous plaques that are prone to becoming culprit plaques and characterized by the accumulation of lipids, inflammatory cell aggregation, and extracellular matrix development.^{1,5-7}

In clinical practice, precise detection of vulnerable plaques is crucial to prevent artery occlusion and provide sufficient evidence for intra-arterial treatments, such as balloon angioplasty and stenting. Several methods are currently employed for detecting atherosclerotic plaques. Ultrasound and optical coherence tomography have proven effective in identifying intima-media protrusions, plaque area, or volume. Computed tomography with an iodine contrast agent can detect and classify plaques into three categories based on their composition: calcified, noncalcified, or a mixture of both.⁸⁻¹⁰ However, the identification of vulnerable atherosclerotic plaques remains a significant challenge. Therefore, there is an urgent need for the development of novel methods capable of accurately identifying vulnerable atherosclerotic plaques.

Biomimetic nanomaterials have recently gained significant attention as contrast agents in the field of medical imaging.¹¹⁻¹⁶ In the context of vulnerable atherosclerotic plaques, platelets adhere to damaged endothelium through interactions involving von Willebrand factor (vWF)-platelet glycoprotein (GP) Ib α , collagen-platelet GPIa-IIa, and GP VI.¹⁷ Given the pivotal spatiotemporal role of platelets in atherosclerosis, the utilization of platelet-inspired agents holds great promise for precise targeting of vulnerable plaques, thereby enhancing imaging efficacy.¹⁸⁻²⁰ Magnetic resonance angiography, employing gadolinium-diethylenetriaminepentaacetic acid as

Key points

- In this work, PM/Fe₃O₄@PLGA were prepared with a W/O/W method, which allowed water-soluble MRI contrast agents to be efficiently loaded and transported in vivo.
- PM/Fe₃O₄@PLGA exhibited the properties of good targeting, biocompatibility, and safety.
- The biomimetic biofilm-coated MRI contrast agents were utilized for diagnosing atherosclerotic vulnerable plaques for the first time.
- PM/Fe₃O₄@PLGA could effectively identify atherosclerotic vulnerable plaques, which showed the potential clinical application value.

a representative agent,²¹ enables accurate assessment of large arteries and veins with high spatial resolution. Notably, Fe₃O₄ has recently emerged as an alternative contrast agent in Magnetic resonance angiography, demonstrating excellent imaging characteristics and a superior safety profile compared to gadolinium-based agents.²²⁻²⁵ In this study, we have developed a novel contrast agent by coating biomimetic Fe₃O₄-based poly(lactic-co-glycolic acid) (PLGA) nanoparticles (Fe₃O₄@PLGA) with a platelet membrane, enabling accurate detection of vulnerable atherosclerotic plaques using magnetic resonance imaging (MRI) T2-weighted images.

In this study, we achieved successful synthesis of PM-coated Fe₃O₄ nanoparticles (PM/Fe₃O₄@PLGA) with a pronounced T2 effect. Subsequent in vitro experiments were conducted to evaluate the physiological functionalities of the PM/Fe₃O₄@PLGA. Additionally, the PM/Fe₃O₄@PLGA exhibited successful detection of vulnerable plaques in an experimental mouse model utilizing MRI. The development of this novel biomimetic contrast

agent holds promising clinical applications in the diagnosis of vulnerable atherosclerotic plaques.

2 | RESULTS AND DISCUSSION

2.1 | Platelets were the best candidate for adherent vulnerable plaques

In recent years, nano-drug delivery systems based on natural biofilms (macrophage, neutrophil and platelet membranes) have been progressively applied in the treatment of various cardiovascular diseases, especially atherosclerosis. However, it is still uncertain which biofilm is the best candidate for nano-diagnostics and therapeutics for atherosclerotic vulnerable plaques. The biological interactions and adhesion between atherosclerotic vulnerable plaque and biofilm are important factors in selecting the optimal biofilm. Therefore, a comprehensive analysis was conducted to explore the potential candidate targeting atherosclerotic vulnerable plaques for nano-diagnostics (Figure 1A). Based on atherosclerotic vulnerable plaque characteristics, a total of 1592 vulnerable atherosclerotic plaques-related genes, 1598 genes related to plaque erosion, 2173 genes related to plaque rupture, and 3056 genes related to thin collagen cap were extracted from GENECARDS (<https://www.genecards.org/>). These datasets were imported into Hiplot (<https://hiplot.com.cn/home/index.html>). 479 common genes were identified and displayed in Venn diagrams (Figure 1B). In addition, a total of 8354, 12,829 and 12,395 genes were extracted based on platelet adhesion, macrophage adhesion and neutrophil adhesion. In order to explore the optimal biofilm for adhesion to vulnerable plaques, the adhesion genes of these different kinds of cells were compared with the common genes that characterize vulnerable plaques, from which we found that they have 427, 430, and 430 genes in common, respectively. 5.1%, 3.35% and 3.47% of their respective total gene counts, respectively (Figure 1C,E,G). Further, we performed GO pathway enrichment analysis on these overlapping genes using the cluster Profiler R package. Figure 1D,F,H show the 10 most relevant pathways in each group. Of the 10 pathways of platelet adhesion, a total of 5 are all associated with adhesion, namely leukocyte cell-cell adhesion, cell adhesion, cell adhesion mediated by integrin, cell-cell adhesion and cell-matrix adhesion. In addition, the top three pathways were also associated with adhesion. Of the overlapping genes for macrophage adhesion and neutrophil adhesion, only three were associated with the adhesion pathway. These findings showed that platelets were the best candidates for adherent vulnerable plaques.

2.2 | Syntheses and characteristics of the platelet-coated Fe₃O₄ nanoparticles

As mentioned above, the platelet membrane (PM) was selected as an optimal coating membrane candidate due to its inherent affinity for vulnerable plaques and its natural presence in atherosclerotic lesions (Figure 2B).^{26,27} To prepare PM/Fe₃O₄@PLGA, Fe₃O₄-loaded PLGA nanoparticles (Fe₃O₄@PLGA) were initially synthesized, followed by coating the Fe₃O₄@PLGA with the PM using an extrusion method (Figure 2A). Dynamic light scattering (DLS) analysis revealed that the diameter of the nanoparticles increased from approximately 244.13 to 280.33 nm after the PM coating step, corresponding to the thickness of the bilayer membrane (Figure 2C). The zeta potentials of the PM and PM/Fe₃O₄@PLGA were measured as -17.2 ± 0.67 and -27.36 ± 1.84 mV, respectively, which suggests prolonged blood circulation compared to nanoparticles with neutral or positive surface charges (Figure 2D). Transmission electron microscopy (TEM) further confirmed the “core-shell” structure of the PM/Fe₃O₄@PLGA (Figure 2E).

To assess the coating of nanoparticles with the platelet membrane, 1,1'-Diocadecyl-3,3,3',3'-tetramethylindocarbocyanine perchlorate (DiI) fluorophore was incorporated into the PLGA “core” instead of Fe₃O₄, while the platelet membrane was labeled with 3,3'-dioctadecyloxocarbocyanine perchlorate (DiO). Confocal laser scanning microscopy (CLSM) analysis demonstrated the colocalization of DiI-labeled PLGA “core” and DiO-labeled platelet membrane, confirming the successful coating of the platelet membrane on the DiI nanoparticles following the extrusion process (Figure S2, Supporting Information). At the site of vulnerable atherosclerotic plaques, ECs were significantly activated, and their adhesion ability was greatly enhanced, enabling them to effectively first contact and adhere PM/DiI@PLGA at the site of vulnerable atherosclerotic plaques. To further investigate the stability of the platelet membrane-coated DiI nanoparticles (DiI@PLGAPM/DiI@PLGA) within target cells after endocytosis, DiO-labeled DiI@PLGAPM/DiI@PLGA were incubated with human umbilical vein endothelial cells (ECs) for 4 h. The majority of DiI and DiO signals were observed to colocalize within the cells (Figure 2F), indicating the robust stability of the PM/Fe₃O₄@PLGA following internalization by the cells. Collectively, these findings provide evidence for the successful coating of PLGA cores with the extracted platelet membrane.

Next, we sought to test the key physiological functions of PM/Fe₃O₄@PLGA inherited from the platelet membrane. Western blot analysis was performed to detect specific protein signals of GP-IIbIIIa, GP-IaIIa, and GP-Ib,

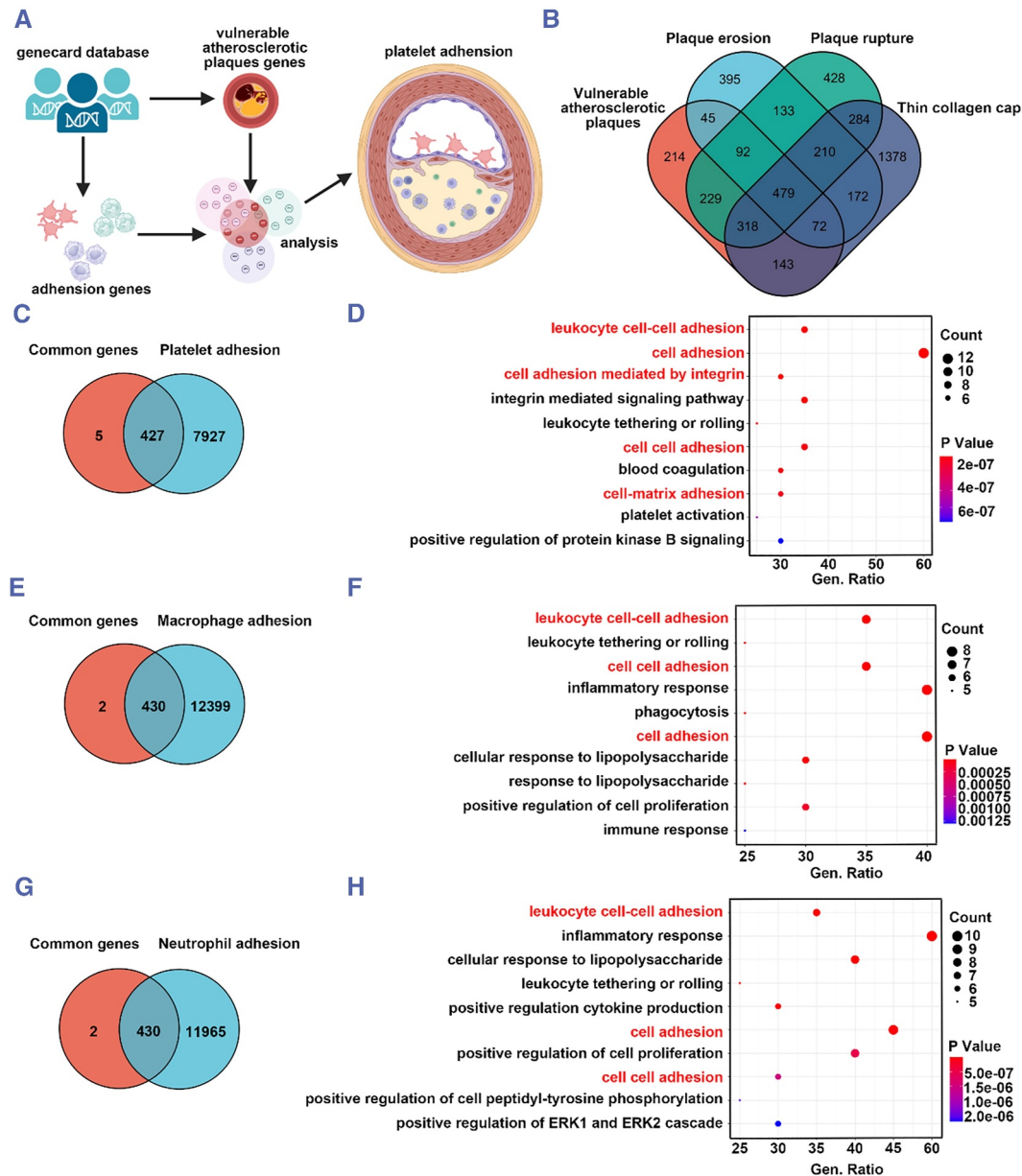


FIGURE 1 Platelets were the best candidates for adherent vulnerable plaques. (A) Schematic diagram of comprehensive analysis of best candidate adhesion to for vulnerable atherosclerotic plaques. (B) Venn diagrams of vulnerable atherosclerotic plaques, plaque erosion, plaque rupture, and thin collagen cap related gene from GENCARDS. Venn diagrams of vulnerable atherosclerotic plaque common genes and Platelet Adhesion (C), Macrophage adhesion (E), and Neutrophil adhesion (G), respectively. GO pathway enrichment analysis of the overlap genes from Platelet adhesion (D), Macrophage adhesion (F), and Neutrophil adhesion (H).

which are crucial for platelet adhesion to injured tissue. The presence of these specific protein signals confirmed the preservation of platelet function on the PM/Fe₃O₄@PLGA following membrane coating (Figure 2G). In addition, the protein composition of Fe₃O₄@PLGA, platelet membrane and PM/Fe₃O₄@PLGA were also shown by Ponceau dyeing (Figure S1). Furthermore, to assess the feasibility of Fe₃O₄ as an MRI contrast agent, T1 and T2 relaxation values of Fe₃O₄ at various Fe₃O₄ concentrations were measured. T1 and T2 relaxation values showed that the ratio of r2 to r1 was relatively high for the

PM/Fe₃O₄@PLGA (PM/Fe₃O₄@PLGA: r2/r1 = 684.81, r2/r1 > 10), indicating a strong T2 effect (Figures 2H,I).

2.3 | Imitating platelet adhesive characteristics in vitro

The targeting of platelets to disease sites involves the interaction between multiple substrates and adhesive factors present on platelet membranes. In this study, we assessed the adhesive properties of the DiI@PLGAPM/

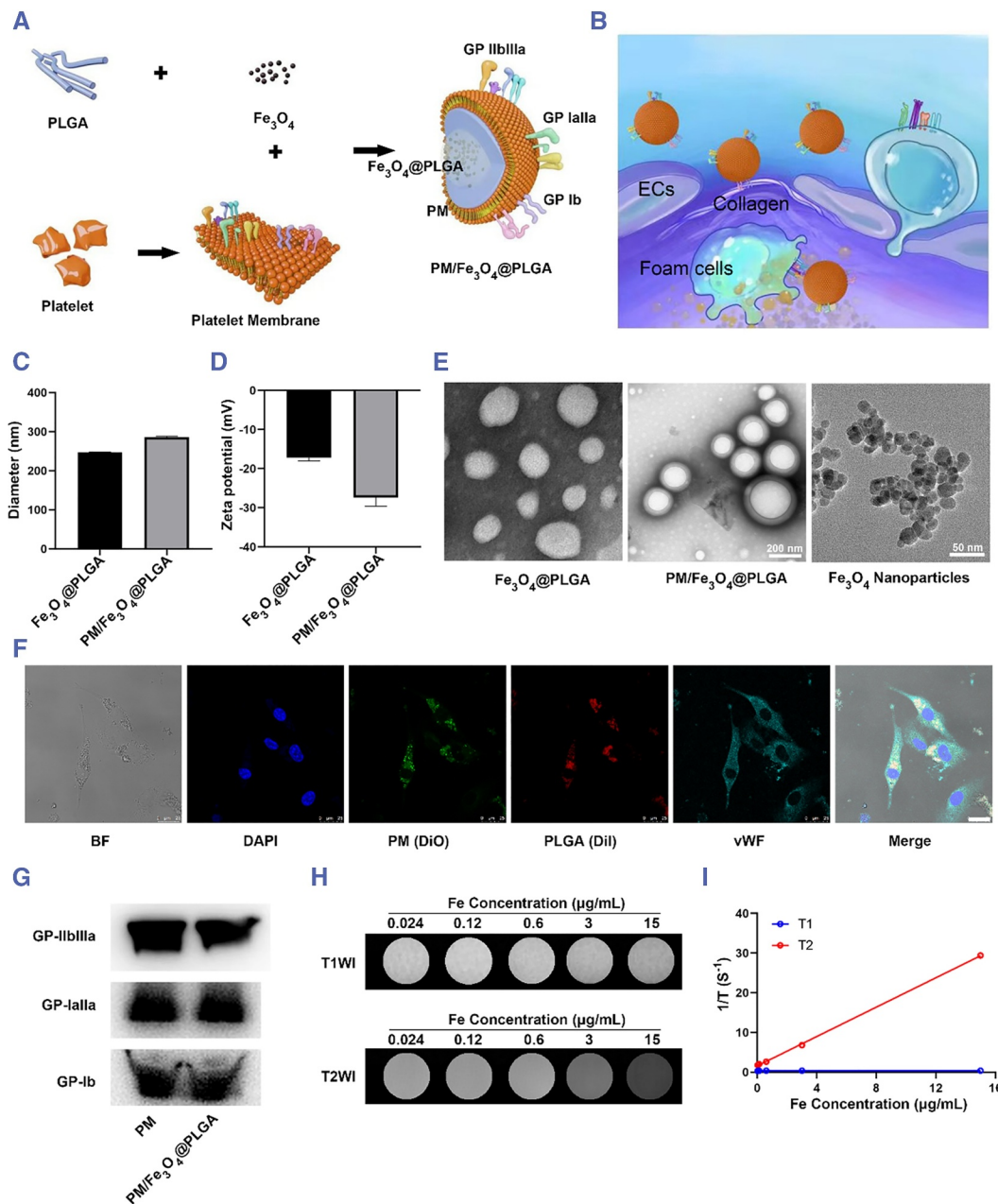


FIGURE 2 Preparation and characterization of PM/Fe₃O₄@PLGA. (A) Schematic illustration of the preparation of PM/Fe₃O₄@PLGA. The membrane of platelet was extracted using a hypotonic lysis method. PM and Fe₃O₄@PLGA were mixed and extruded to formulate PM/Fe₃O₄@PLGA. (B) Schematic diagram of vulnerable atherosclerotic plaque targeting performance of PM/Fe₃O₄@PLGA in the blood vessels. (C) Particle size of Fe₃O₄@PLGA and PM/Fe₃O₄@PLGA measured by DLS. (D) Zeta potential distribution of Fe₃O₄@PLGA and PM/Fe₃O₄@PLGA. (E) TEM images of Fe₃O₄@PLGA and PM/Fe₃O₄@PLGA. (Scale bar = 100 nm). (F) CLSM images of ECs after incubation with PM/Fe₃O₄@PLGA for 4 h. The nuclei of ECs were stained with DAPI. The PM “shell” was labelled with DiO and the PLGA core was labelled with DiI. The merged image is the overlay of the four individual images (Scale bar = 25 μm). (G) Representative protein bands of PM and PM/Fe₃O₄@PLGA measured by western blot. (H) MRI images of different concentration aqueous solutions of PM/Fe₃O₄@PLGA. (I) T1 and T2 relaxation times of PM/Fe₃O₄@PLGA.

DiI@PLGA by examining their ability to bind to collagen and von Willebrand factor (vWF), as well as their uptake by foam cells in vitro. To evaluate the binding ability of the DiI@PLGA to collagen, a flow chamber study was conducted at a shear rate of 500/s. The results

demonstrated that the PM/DiI₄ NPs exhibited significant adhesion to collagen, whereas the DiI@PLGA showed minimal binding to collagen (Figure 3A). To evaluate the binding efficacy of PM/NPs to von Willebrand factor (vWF), human umbilical vein endothelial cells (HUVECs)

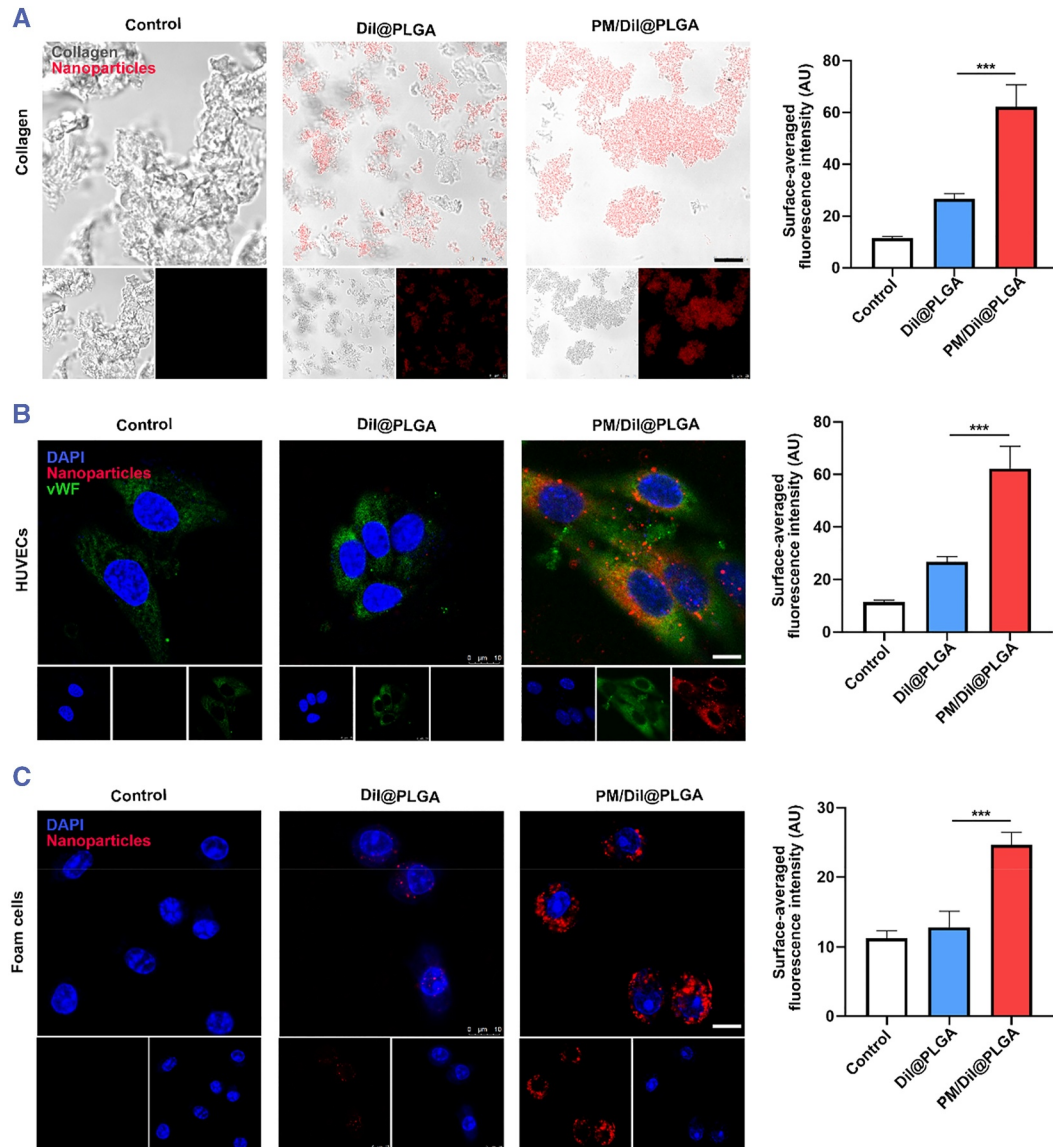


FIGURE 3 Targeted delivery performance of PM NPs. (A) The ability of collagen adheres with DiI@PLGA and PM/DiI@PLGA after 4 h incubation with in vitro collagen (gray is collagen, red is encapsulated DiI fluorescent molecules, scale bar = 10 μ m). (B) Cell uptake of DiI NPs and PM/DiI NPs after incubation with foam cells for 4 h. The nuclei of foam cells were stained with DAPI (scale bar = 10 μ m). (C) Cell uptake of DiI NPs, MM/DiI NPs and MMM/DiI NPs after incubation with activated HUVECs (stimulated with TNF- α) for 4 h. The nuclei of HUVECs were stained with DAPI (scale bar = 10 μ m). (Mean \pm SD, $n = 3$ independent experiments). *** $p < 0.001$, one-way ANOVA, Tukey's multiple comparison test.

were stimulated with Recombinant human Tumor Necrosis Factor (TNF- α) to induce vWF expression. Subsequently, the cells were treated with DiI@PLGAPM/DiI@PLGA and DiI@PLGA for 4 h. The PM/DiI NP group exhibited strong red fluorescence signals on the cell surface, whereas only green fluorescence corresponding to vWF was observed in the non-targeted DiI NP group (Figure 3B).

Platelets play a crucial role in guiding inflammatory cells to atherosclerotic vulnerable plaques through the formation of platelet-mononuclear complexes, which

can be taken up by foam cells. Therefore, we examined the cellular uptake of DiI@PLGAPM/DiI@PLGA by foam cells in vitro. RAW 264.7 cells were treated with Ox-LDL to stimulate foam cell formation. Fluorescence imaging demonstrated a significantly higher accumulation of DiI@PLGAPM/DiI@PLGA within foam cells compared to DiI@PLGA (Figure 3C). These results suggest that DiI@PLGAPM/DiI@PLGA exhibit adhesive properties similar to platelets, thereby facilitating their targeted binding to vWF and uptake by foam cells.

2.4 | Detection of vulnerable atherosclerotic plaques by PM/Fe₃O₄@PLGA in vivo

To investigate the capability of PM/Fe₃O₄@PLGA in detecting vulnerable atherosclerotic plaques, a mouse model of atherosclerosis characterized by plaque instability/rupture was established (Figure 4A). Coarctation surgery was performed on the left carotid artery (LCA) of mice, while the right carotid arteries (RCA) remained untreated. The induction of vulnerable plaques in the LCA was facilitated by a high-fat diet, whereas stable atherosclerotic plaques were observed in the RCA. In this study, ApoE^{-/-} mice with vulnerable atherosclerotic plaques were administered PM/Fe₃O₄@PLGA or Fe₃O₄@PLGA (0.72 mg/kg Fe) via the tail vein. MRI was conducted over a 24-h period to visualize the vulnerable atherosclerotic plaques in the mouse carotid artery (Figure 4A). Transverse plane images revealed a distinct MR signal in the LCA of the atherosclerotic mouse that received PM/Fe₃O₄@PLGA 24 h post-injection, while no significant changes in the MR signal were observed in

atherosclerotic mice treated with Fe₃O₄@PLGA. Additionally, no signal was detected in the RCA of either treatment group (Figure 4C–E). These findings indicate the specific targeting ability of PM/Fe₃O₄@PLGA towards vulnerable atherosclerotic plaques in vivo.

Furthermore, to assess the diagnostic potential of PM/Fe₃O₄@PLGA in identifying vulnerable plaques, 25 ApoE^{-/-} mice with vulnerable atherosclerotic plaques underwent MRI, yielding an area under the curve (AUC) of 0.954 ± 0.026 . Receiver Operating Characteristic (ROC) analyses revealed an optimal cutoff of 8493.5, resulting in 88% sensitivity and 88% specificity (Figure 4B). These results demonstrate the excellent diagnostic efficacy of PM/Fe₃O₄@PLGA for vulnerable atherosclerotic plaques in vivo.

2.5 | Targeting effect of PM/Fe₃O₄@PLGA to vulnerable plaque

Subsequently, we assessed the in vivo targeting capability of PM nanoparticles towards vulnerable plaques in

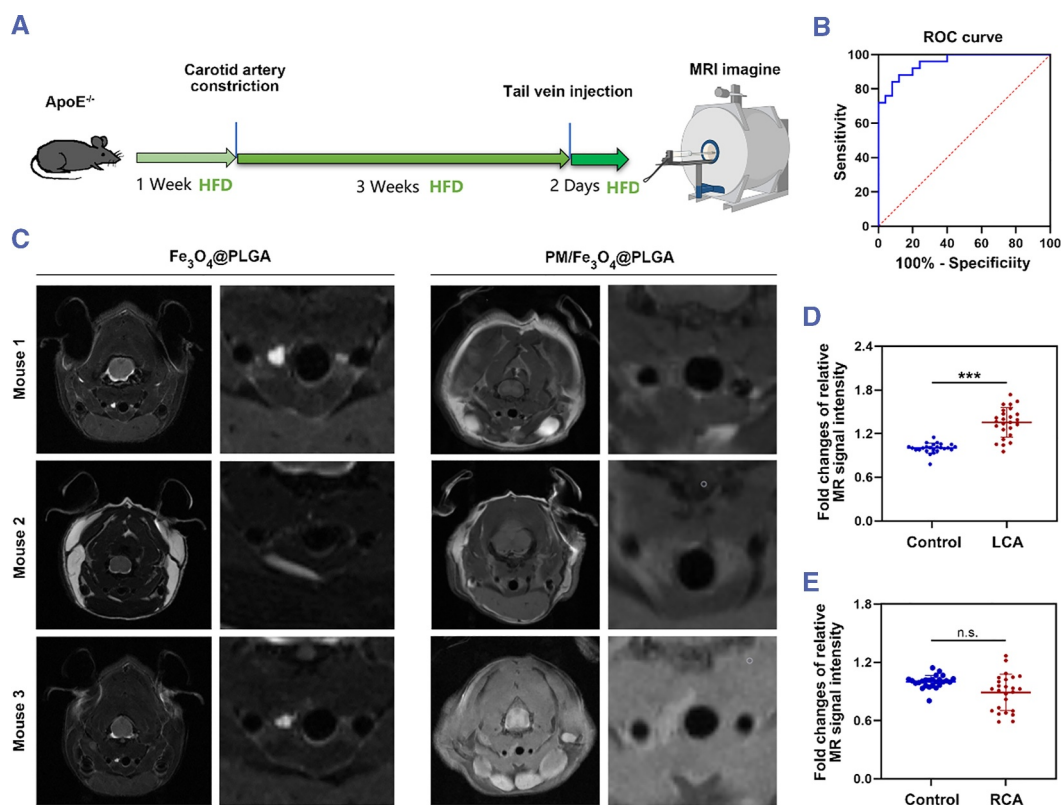


FIGURE 4 MRI of the vulnerable atherosclerotic plaque in vivo. (A) Experiment setup in this study. (B) Receiver Operating Characteristic (ROC) curve showing the performance of different plaques (stable plaque, venerable plaque) in terms of true positive rate and false positive rate. (C) MRI images were taken 24 h after injection. Red arrows point to atherosclerosis vulnerable plaque ($n = 25$). (D, E) Quantitative analysis of relative MR signal intensity in atherosclerotic mice treated with PM/Fe₃O₄@PLGA was conducted through a RadiAnt DICOM Viewer (mean ± SD, $n = 25$ independent experiments). *** $p < 0.001$, LCA, left carotid artery; n.s., not significant; RCA, right carotid artery; t test.

a mouse model by histological analysis. For CLSM analysis, DiI@PLGAPM/DiI@PLGA was employed. An equal number of DiI@PLGA and DiI@PLGAPM/DiI@PLGA were intravenously injected into mice with vulnerable atherosclerotic plaques. Frozen sections of the plaques in the LCA and RCA were examined 24 h post-injection. Minimal fluorescence signal was observed in the vulnerable plaque following injection of DiI@PLGA in the LCA, whereas sections from PM/DiI-NP-treated mice exhibited abundant fluorescence signal, indicating enhanced targeting of the vulnerable plaque by PM NPs (Figure 5A,B). In addition, H&E, Oil Red O and Masson-stained RCA and LCA are also shown in Figure 5C,D.

Here, DiI@PLGAPM/DiI@PLGA was shown to effectively accumulate in these regions through CLSM analysis. Meanwhile, *in vivo* MRI of the mice confirmed the ability of the PM/Fe₃O₄@PLGA to recognize atherosclerotic vulnerable plaques above. These findings could lead to the identification of vulnerable atherosclerotic plaques for clinical diagnosis.

2.6 | Biosafety assignment

To assess the potential biological impact of PM nanoparticles, we exposed ECs, smooth muscle cells (SMCs) and macrophages to the PM nanoparticles, as well as to PLGA nanoparticles. The cytotoxicity of these materials was evaluated using the Cell Counting Kit-8 (CCK-8) assay. As depicted in Figure S3, no significant differences were observed between the various treatment groups and the control group that was not exposed to any nanoparticles. These findings indicate that our drug delivery system is well tolerated by cells and exhibits favorable cytocompatibility.

Moreover, blood compatibility tests demonstrated that the different PLGA nanoparticles and PM NPs did not induce significant hemolysis (Figure S4). These results further support the good biocompatibility and biosafety of the prepared PM NPs.

In vivo, histological examination of various organ sections using H&E staining revealed no notable differences between the control group and the different

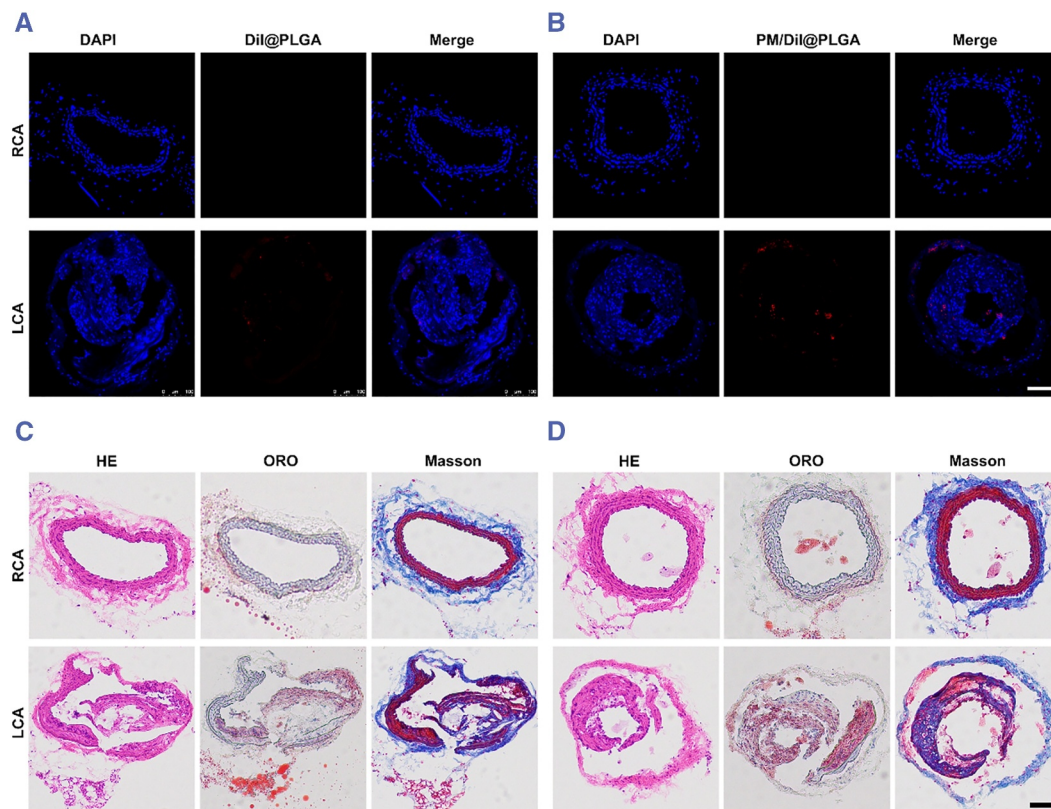


FIGURE 5 PM NPs mediated delivery to the vulnerable atherosclerotic plaque mice and H&E, Oil Red O and Masson-stained vulnerable atherosclerotic plaque. (A), (B) CLSM images of different DiI labelled nanoparticles in atherosclerotic plaque of LCA and RCA in the vulnerable atherosclerotic plaque mice at 24 h post intravenous injection (scale bar = 100 μm). The cell nuclei were stained with DAPI and different nanoparticles were labelled with DiI. (C), (D) H&E, Oil Red O and Masson-stained vulnerable atherosclerotic plaque (scale bar = 100 μm). LCA, left carotid artery; RCA, right carotid artery.

treatment groups of mice with vulnerable atherosclerotic plaques (Figure S5). Furthermore, analysis of cytokine levels (TNF- α , Interleukin-1 β (IL-1 β), Interleukin-6 (IL-6), and C-C motif chemokine ligand 2 (CCL2)) in mouse serum did not display any significant differences between the treatment groups and the control group (Figure S6). These findings suggest that PM/Fe₃O₄@PLGA and Fe₃O₄@PLGA exhibit high biocompatibility after long-term treatment in mice with vulnerable atherosclerotic plaques.

3 | CONCLUSIONS

In the present study, we have successfully developed a nanoparticle system coated with platelet membranes for the targeted delivery of Fe₃O₄ nanoparticles to vulnerable atherosclerotic plaques, enabling the visualization of these plaques through MRI. Western blot indicated that the key proteins on the platelet membrane surface that mediate adhesion to collagen are not lost during the membrane extraction and re-encapsulation process *in vitro*. Furthermore, functional experiments provided further evidence that the platelet membrane encapsulated on the NPs retained its ability to adhere to collagen and induce macrophage cellular uptake. This novel formulation was also found to be a safe and effective *in vivo* MRI contrast agent.

In this study, the results demonstrated that PM/Fe₃O₄ nanoparticles exhibited excellent biocompatibility and possessed the ability to target atherosclerosis-prone plaque lesions. A major advantage of our PM NP delivery system is the advanced targeting ability in response to biological signals in the process of vulnerable atherosclerosis compared to the traditional nanoparticle delivery system. This innovative approach expands the application of biomimetic platelet membrane-modified nanoparticles and holds great potential for clinical diagnosis of vulnerable atherosclerotic plaques.

4 | EXPERIMENTAL SECTION

Materials and Cells: The anti-human vWF antibody was bought from Abclonal (Changsha, China), and the anti-mouse GP-Iba antibody was obtained from ProMab (USA). PLGA (75:25; MW = 20,000) and an aqueous solution of Fe₃O₄ particles were purchased from Dalian Meilun Biotechnology (Dalian, China). Polyvinyl alcohol (PVA) (MW = 30,000–70,000) was purchased from Aladdin Bio-Chem Technology (Shanghai) Co., Ltd. (Shanghai, China). DiI and DiO were purchased from

Beyotime (Beijing, China). TNF- α was purchased from Novoprotein Scientific. Inc. (Canada). Servicebio (Wu Han, China) provided hematoxylin and eosin, Masson's trichrome, and Oil Red O (ORO). Ponceau S, a Cell Counting Kit 8 (CCK-8) and a Bicinchoninic Acid Assay (BCA) protein assay kit were purchased from Biosharp (China). Mouse TNF- α and IL-6 ELISA kit was purchased from LunchangshuoBiotech (Xiamen, China). Mouse CCL2 ELISA kit was purchased from Fankew (Shanghai, China) and mouse IL-1 β ELISA kit was purchased from Jingmei Biological Technology Co.,Ltd (Jiangsu, China).

The murine RAW 264.7 cell line, the murine SMCs and HUVECs were purchased from Beinart Biotech (Beijing, China).

Construction of Pathways. Vulnerable atherosclerotic plaques-related genes and cell adhesion genes were retrieved from GeneCards (<https://www.genecards.org/>). Vene diagrams showing common genes were designed in Hiplot (<https://hiplot.com.cn/home/index.html>). The common gene profiles were analyzed using the bio-conductor packet. R were used for GO enrichment analysis.

Isolation of the PM. The platelet membrane was generated using a repeated freeze–thaw process as previously described.²⁸ The platelets were subjected to hypotonic lysis to extract a biologically active membrane. The hypotonic lysate solution was prepared as previously described.²⁹ The protein concentration was measured using the BCA protein assay kit.

Preparation of Fe₃O₄@PLGA: We employed the nanoprecipitation method to fabricate Fe₃O₄ nanoparticles, following a previously established protocol. In summary, we dissolved 100 mg of PLGA in dichloromethane and then added 0.2 mL of an aqueous solution containing Fe₃O₄ particles (1 mg/mL). The mixture underwent 60 s of acoustic vibration using an ultrasonic oscillation instrument, resulting in the formation of a brown emulsion. The emulsion was homogenized at 15,000 rpm for 5 min in a 10 mL 3% PVA solution using a high-speed homogenization dispersion machine. The nanoparticle surface solidified as dichloromethane was volatilized over 2 h at room temperature, followed by the addition of 20 mL of a 2% isopropanol solution. Similarly, DiI-labeled NPs were prepared in the same manner but with the inclusion of 0.1 wt% DiI.

Preparation of PM/Fe₃O₄@PLGA: To prepare platelet membrane vesicles, the extracted membrane was sonicated for 20 min. After mixing the platelet vesicles with Fe₃O₄@PLGA, sonicating, and extruding through 200 nm-pore membrane filters, the pellets were reconstituted.

The hydrodynamic size of Fe₃O₄ nanoparticles as well as the zeta potential of PM/Fe₃O₄ nanoparticles

were measured using DLS (Malvern Panalytical, England). Morphologies were determined by TEM (FEI Tecnai F20, America).

Flow chamber experiment for collagen binding analysis: A microscope slide was coated with 20 μL of collagen solution type IV (2.0 mg/mL in 0.25% acetic acid) at 4°C. Flow chambers were then filled with DiI-labeled PM/Fe₃O₄ or Fe₃O₄@PLGA (5×10^6 /mL) suspended in PBS for 3 min, followed by a 5-min washing period. CLSM (Leica, Germany) was used to measure nanoparticle adhesion to collagen.

Cell uptake in vitro: RAW 264.7 cells were treated with Ox-LDL to stimulate foam cell formation. The cells were cultured overnight. DiI@PLGA and DiI@PLGAPM/DiI@PLGA (150 μg per well) were added and cultured for 4 h. Subsequently, the cell nuclei were stained with DAPI and observed using CLSM.

Following exposure to 50 ng/mL TNF- α (Gibco) for 24 h, the HUVECs were treated with either 100 μg of DiI@PLGA or PM/DiI NPs, depending on their activation status. After 2 h of incubation, the uptake efficiencies of the DiI@PLGAPM/DiI@PLGA were measured using CLSM. The cell nuclei were stained with DAPI and analyzed using CLSM.

Cytotoxicity test: The types of cells were plated in a 96-well plate at a density of 1×10^4 cells/well and allowed to incubate for about 6 h. Subsequently, the cells were treated with PM/NPs for 24 h, and cell viability was assessed using CCK-8 assays.

Blood compatibility tests: One milliliter of sodium chloride solution was obtained by diluting with 1.25 mL of rat blood. Subsequently, 100 μL of diluted whole blood was added to a 5 mL solution of Fe₃O₄@PLGA or PM/Fe₃O₄@PLGA and incubated for 1 h at 37°C, followed by centrifugation at 3000 rpm for 5 min. The release of hemoglobin from lysed red blood cells was measured from the supernatant at 540 nm.

Mice and Treatments: The ApoE^{-/-} mice were raised at the First Affiliated Hospital of Anhui Medical University's Experimental Animal Center.

Mice were first adapted to high-fat feeding for 1 week before surgery, narrowing their LCA.³⁰ An adaptation period of 3 weeks was then used to establish a model of vulnerable plaque in mice fed a high-fat diet. PBS, Fe₃O₄@PLGA, and PM/Fe₃O₄@PLGA were injected intravenously into mice 4 weeks after carotid artery constriction. LCA and RCA atherosclerotic lesions were detected via MRI after 24-h.

Recognition of vulnerable plaques in vivo: Using a tail vein injection, mice bearing atherosclerosis-vulnerable plaques were administered PBS, Fe₃O₄ nanoparticles, or PM/Fe₃O₄ nanoparticles (0.72 mg/kg Fe). In order to

illustrate the cross sections of the LCA and RCA, MRI using a T2-weighted sequence was performed using a BioSpec94/20 MRI scanner (echo time (TE):30 ms; repetition time (TR):3000 ms; Field of View (FOV) 25 mm \times 25 mm; resolution 110 μm \times 110 μm ; slice Thickness 0.8 mm).

H&E and Masson staining: Under anesthesia, the mice LCA and RCA were carefully dissected, washed and fixed after sacrifice. For quantification of atherosclerotic lesions, the LCA and RCA were stained with ORO. For assessment of atherosclerotic plaque stability, Masson's trichrome was used on the LCA and RCA. The images were captured using OLYMPUS imaging software.

Evaluation of inflammatory factors: For assessing the inflammatory factors after MRI, mice were euthanized. Mouse serum was collected and inflammatory factors were detected using the ELISA kits.

Statistical analysis: The data are presented as the mean \pm SEM. Statistical analysis was carried out using GraphPad Prism. One-way analysis of variance (ANOVA) was utilized for data analysis. The significance level was defined as * $p < 0.001$, ** $p < 0.01$ and *** $p < 0.001$.

AUTHOR CONTRIBUTIONS

Conceptualization: Jun Xie and Yuyu Li; Methodology: Yuyu Li, Yujie Wang and Zequn Xia; Investigation: Yuyu Li, Daozheng Ke, Bing Song, Dan Mu and Ronghui Yu; Writing-Original Draft: Yuyu Li; Funding Acquisition: Jun Xie; Resources: Dan Mu, Ronghui Yu and Jun Xie; Supervision: Yuyu Li and Jun Xie.

ACKNOWLEDGMENTS

The authors would like to thank Dr. Jiaqi Yu, Dr. Weiyao Chen and Dr. Yanyan Gong for technical support and scientific advice. The authors wanted to thank the staff of PROMAB for some technique support. This work was supported by grants from the National Natural Science Foundation of China (92068116 and 82370305) and the Science Fund for Distinguished Young Scholars in Jiangsu Province (grant number BK20211501).

CONFLICT OF INTEREST STATEMENT

The authors declare that they have no competing interests.

ETHICS STATEMENT

All procedures with animals were approved by the Institution Ethics Committee of Anhui Medical University (Anhui, China) (No. LLSC20230846) and performed in accordance with the guidelines from Directive 2010/63/EU of the European Parliament.

ORCID

Jun Xie  <https://orcid.org/0000-0002-9385-3242>

REFERENCES

1. P. Libby, *Nature* **2021**, 592, 524.
2. K. Kobiyama, K. Ley, *Circ. Res.* **2018**, 123, 1118.
3. W. Herrington, B. Lacey, P. Sherliker, J. Armitage, S. Lewington, *Circ. Res.* **2016**, 118, 535.
4. Y. Li, Y. Zhang, J. Lu, Y. Yin, J. Xie, B. Xu, *J. Cell. Mol. Med.* **2021**, 25, 8087.
5. P. Gaba, B. J. Gersh, J. Muller, J. Narula, G. W. Stone, *Nat. Rev. Cardiol.* **2023**, 20, 181.
6. S. Zhang, Y. Liu, Y. Cao, S. Zhang, J. Sun, Y. Wang, S. Song, H. Zhang, *Adv. Mater.* **2022**, 34, 2110660.
7. J. F. Bentzon, F. Otsuka, R. Virmani, E. Falk, *Circ. Res.* **2014**, 114, 1852.
8. A. N. Nicolaides, A. G. Panayiotou, M. Griffin, T. Tyllis, D. Bond, N. Georgiou, E. Kyriacou, C. Avraamides, R. M. Martin, *J. Am. Coll. Cardiol.* **2022**, 79, 1969.
9. P. Joseph, A. Tawakol, *Eur. Heart J.* **2016**, 37, 2974.
10. T. Emrich, M. Hell, *Eur. Heart J.* **2023**, 44, 1765.
11. P. Zhang, Y. Qiao, L. Zhu, M. Qin, Q. Li, C. Liu, Y. Xu, X. Zhang, Z. Gan, Y. Hou, *ACS Nano* **2023**, 17, 184.
12. L. Dong, Y. J. Xu, C. Sui, Y. Zhao, L. B. Mao, D. Gebauer, R. Rosenberg, J. Avaro, Y. D. Wu, H. L. Gao, Z. Pan, H. Q. Wen, X. Yan, F. Li, Y. Lu, H. Cölfen, S. H. Yu, *Nat. Commun.* **2022**, 13, 5088.
13. W. Yang, C. Xiang, Y. Xu, S. Chen, W. Zeng, K. Liu, X. Jin, X. Zhou, B. Zhang, *Biomaterials* **2020**, 255, 120186.
14. P. Zhang, J. Meng, Y. Li, C. Yang, Y. Hou, W. Tang, K. J. McHugh, L. Jing, *Innovation* **2021**, 2, 100174.
15. Q. Zhang, G. Kuang, H. Wang, Y. Zhao, J. Wei, L. Shang, *Adv. Sci.* **2023**, 10, 2303818.
16. M. A. Fardjahromi, H. Nazari, S. M. A. Tafti, A. Razmjou, S. Mukhopadhyay, M. E. Warkiani, *Mater. Today Chem.* **2022**, 23, 100670.
17. H. F. Langer, M. Gawaz, *Thromb. Haemost.* **2008**, 99, 480.
18. Y. Jiang, J. Wang, H. Zhang, G. Chen, Y. Zhao, *Sci. Bull.* **2022**, 67, 1776.
19. Y. Wang, L. Shang, G. Chen, L. Sun, X. Zhang, Y. Zhao, *Sci. Adv.* **2020**, 6, eaax8258.
20. Y. Zhu, L. Sun, Y. Wang, L. Cai, Z. Zhang, Y. Shang, Y. Zhao, *Adv. Mater.* **2022**, 34, 2108972.
21. E. Kanal, M. F. Tweedle, *Radiology* **2015**, 275, 630.
22. H. Wei, O. T. Bruns, M. G. Kaul, E. C. Hansen, M. Barch, A. Wiśniowska, O. Chen, Y. Chen, N. Li, S. Okada, J. M. Cordero, M. Heine, C. T. Farrar, D. M. Montana, G. Adam, H. Ittrich, A. Jasanoff, P. Nielsen, M. G. Bawendi, *Proc. Natl. Acad. Sci. U. S. A.* **2017**, 114, 2325.
23. G. B. Toth, C. G. Varallyay, A. Horvath, M. R. Bashir, P. L. Choyke, H. E. Daldrup-Link, E. Dosa, J. P. Finn, S. Gahramanov, M. Harisinghani, I. Macdougall, A. Neuwelt, S. S. Vasanaawala, P. Ambady, R. Barajas, J. S. Cetas, J. Ciporen, T. J. DeLoughery, N. D. Doolittle, R. Fu, J. Grinstead, A. R. Guimaraes, B. E. Hamilton, X. Li, H. L. McConnell, L. L. Muldoon, G. Nesbit, J. P. Netto, D. Petterson, W. D. Rooney, D. Schwartz, L. Szidonya, E. A. Neuwelt, *Kidney Int.* **2017**, 92, 47.
24. R. F. Barajas, B. E. Hamilton, D. Schwartz, H. L. McConnell, D. R. Pettersson, A. Horvath, L. Szidonya, C. G. Varallyay, J. Firkins, J. J. Jaboin, C. D. Kubicky, A. M. Raslan, A. Dogan, J. S. Cetas, J. Ciporen, S. J. Han, P. Ambady, L. L. Muldoon, R. Woltjer, W. D. Rooney, E. A. Neuwelt, *Neuro-Oncology* **2019**, 21, 517.
25. D. Huang, J. Wang, C. Song, Y. Zhao, *Innovation* **2023**, 4, 100421.
26. M. Gawaz, T. Geisler, O. Borst, *Nat. Rev. Cardiol.* **2023**, 20, 583.
27. Y. Li, J. Wang, J. Xie, *Smart Med.* **2023**, 2, e20230015.
28. Y. Song, Z. Huang, X. Liu, Z. Pang, J. Chen, H. Yang, N. Zhang, Z. Cao, M. Liu, J. Cao, C. Li, X. Yang, H. Gong, J. Qian, J. Ge, *Nanomed. Nanotechnol. Biol. Med.* **2019**, 15, 13.
29. Y. Li, J. Che, L. Chang, M. Guo, X. Bao, D. Mu, X. Sun, X. Zhang, W. Lu, J. Xie, *Adv. Healthcare Mater.* **2022**, 11, 2101788.
30. Y. C. Chen, A. V. Bui, J. Diesch, R. Manasseh, C. Hausding, J. Rivera, I. Haviv, A. Agrotis, N. M. Htun, J. Jowett, C. E. Hagemeyer, R. D. Hannan, A. Bobik, K. Peter, *Circ. Res.* **2013**, 113, 252.

SUPPORTING INFORMATION

Additional supporting information can be found online in the Supporting Information section at the end of this article.

How to cite this article: Y. Li, Y. Wang, Z. Xia, Y. Xie, D. Ke, B. Song, D. Mu, R. Yu, J. Xie, *Smart Med.* **2024**, 3(2), e20240006. <https://doi.org/10.1002/SMMD.20240006>